Results in Physics 9 (2018) 100–112

Contents lists available at ScienceDirect

Results in Physics

journal homepage: www.journals.elsevier.com/results-in-physics

Melamine derivatives as effective corrosion inhibitors for mild steel in acidic solution: Chemical, electrochemical, surface and DFT studies

Chandrabhan Verma [a,b,*], J. Haque [c], Eno E. Ebenso [a,b,*], M.A. Quraishi [d]

[a] Department of Chemistry, School of Mathematical & Physical Sciences, Faculty of Agriculture, Science and Technology, North-West University (Mafikeng Campus), Private Bag X2046, Mmabatho 2735, South Africa
[b] Material Science Innovation & Modelling (MaSIM) Research Focus Area, Faculty of Agriculture, Science and Technology, North-West University (Mafikeng Campus), Private Bag X2046, Mmabatho 2735, South Africa
[c] Department of Chemistry, Indian Institute of Technology, Banaras Hindu University, Varanasi 221005, India
[d] Center of Research Excellence in Corrosion, Research Institute, King Fahd University of Petroleum & Minerals, Dhahran 31261, Saudi Arabia

ARTICLE INFO

Article history:
Received 10 January 2018
Received in revised form 6 February 2018
Accepted 7 February 2018
Available online 23 February 2018

Keywords:
Acid inhibitors
Melamine derivatives
DFT calculations
Langmuir adsorption isotherm
Cathodic inhibitors

ABSTRACT

In present study two condensation products of melamine (triazine) and glyoxal namely, 2,2-bis(4,6-diamino-1,3,5-triazin-2-ylamino)acetaldehyde (ME-1) and (N^2,$N^{2'}$E,N^2,$N^{2'}$E)–N^2,$N^{2'}$-(ethane-1,2-diylidene)-bis-(1,3,5-triazine-2,4,6-triamine) (ME-2) are tested as mild steel corrosion inhibitors in acidic solution (1M HCl). The inhibition efficiency of ME-1 and ME-2 increases with increase in their concentrations and maximum values of 91.47% and 94.88% were derived, respectively at 100 mgL^{-1} (34.20×10^{-5} M) concentration. Adsorption of ME-1 and ME-2 on the surface of metal obeyed the Langmuir adsorption isotherm. Polarization investigation revealed that ME-1 and ME-2 act as mixed type inhibitors with minor cathodic prevalence. The chemical and electrochemical analyses also supported by surface characterization methods where significant smoothness in the surface morphologies was observed in the images of SEM and AFM spectra. Several DFT indices such as E_{HOMO} and E_{LUMO}, ΔE, η, σ, χ, μ and ΔN were derived for both ME-1 and ME-2 molecules and correlated with experimental results. The DFT studies have also been carried out for protonated or cationic form of the inhibitor molecules by considering that in acidic medium the heteroatoms of organic inhibitors easily undergo protonation. The experimental and density functional theory (DFT) studies (neutral and protonated) were in good agreement.

Introduction

Acidic solutions are widely employed in descaling, pickling, cleaning and oil acidification procedures through which damage of metallic resources occur by corrosion [1,2]. Therefore, these procedures required implementation of some additives identified as corrosion inhibitors to avoid the corrosive dissolution of metals [3,4]. Among the previously employed methods, implementation of organic compounds is one of the best practices to avoid corrosion. These compounds contain heteroatoms (P, N, O and S) in form of polar functional groups such as —SO_3H, —COOH, —NH_2, —NO_2, —OH, —OCH_3, —$CONH_2$ and —$COOC_2H_5$ etc. through which they can effectively adsorb and form surface protective films [5–8]. More so, these compounds contain extensive conjugation in form of multiple bonds and non-bonding electrons can also act as adsorption centers. However, the application of these inhibitors is inadequate solubility in polar aggressive solution due to their highly hydrophobic nature [4,6–8]. Literature study revealed that nitrogen containing heterocyclic compounds exhibit good protection ability due to the formation of co-ordinate bonds between unshared electron pairs of nitrogen and d-orbital of superficial iron (Fe) atoms.

Melamine is well established nitrogen rich triazine ring containing molecule with three additional nitrogen atoms those can easily protonate and enhance the solubility of polar solvents [9]. Recently, derivatization of melamine gained the significant advanced for variety of purposes including corrosion inhibition. Literature survey revealed that melamine and its several derivatives have been investigated as effective corrosion inhibitors for metals and alloys in aggressive solutions owing to their high protection ability which is in turn attributed to the adsorption of these compounds by their protonizable amino groups and non-bonding electrons of nitrogen atoms and π-electrons of three double (—C═N—) bonds [10–13].

* Corresponding authors at: Department of Chemistry, School of Mathematical & Physical Sciences, Faculty of Agriculture, Science and Technology, North-West University (Mafikeng Campus), Private Bag X2046, Mmabatho 2735, South Africa.
E-mail addresses: chandraverma.rs.apc@itbhu.ac.in (C. Verma), Eno.Ebenso@nwu.ac.za (E.E. Ebenso).

https://doi.org/10.1016/j.rinp.2018.02.018
2211-3797/

Recently, Liao and coworkers [9] demonstrated the effect of five melamine derivatives designated as T_1, T_2, T_3, T_4 and T_5 having either one or three identical nitrogen containing alkyl chain(s). The study was performed using DFT and several experimental methods such as weight loss, surface (SEM) and electrochemical (EIS, PDP) methods. Results showed that protection power of these inhibitors increases with increasing the hydrophobicity (length of alkyl chain(s)). The melamine derivatives having greater number and larger size of hydrophobic chains show higher protection ability as compared to their other derivatives having smaller number and fewer sizes of hydrophobic chains. Beside this several other derivatives of melamine have also been explored as corrosion inhibitors. Therefore, the development and implementation of new melamine derivatives as corrosion inhibitors is highly anticipated owing to the high solubility and high protection ability of melamine derivatives as compared to the melamine itself. In view of this, present investigation deals with the implementation of two new melamine derivatives synthesized by condensation of melamine and glyoxal and demonstrated as corrosion inhibitors for acidic (1M HCl) corrosion of mild steel for the first time. Several commonly employed methods such as chemical (weight loss), electrochemical impedance spectroscopy (EIS), potentiodynamic polarization (PDP), atomic force microscope (AFM) and scanning electron microscopy (SEM) have been undertaken to study the inhibition ability of the melamine derivatives. The adsorption and inhibition behavior of ME-1 and ME-2 were supported by density functional theory (DFT) based quantum chemical calculations method. A significant correlation among the parameters of experimental and theoretical methods has been achieved in present study.

Experimental sections

Materials

The 2,2-bis-(4,6-diamino-1,3,5-triazin-2-ylamino)acetaldehyde (ME-1) and (N2,N2′E,N2,N2′E)–N2,N2′-(ethane-1,2-diylidene)bis(1,3,5-triazine-2,4,6-triamine) (ME-2) tested as corrosion inhibitors in the study was synthesized as per the reported literature [14]. The synthetic scheme for ME-1 and ME-2 has been given in Fig. 1 and information data are presented in Table 1. Corrosion inhibition tendency of ME-1 and ME-2 has been tested in 1M hydrochloric acid medium. The mild steel sheet with percentage with wt.% configuration of Si (0.026%), Cr (0.05%), P (0.012%), C (0.076%), Mn (0.192%), Al (0.023%) and Fe (99.621%) was chosen as test material. The test electrolyte solution was 1M HCl that was prepared by watering of analytical grade 37% HCl (MERCK) by deionized water. Prior to the experiments, the test specimens were abraded to remove the scales and rusts collected over the surface with the emery papers ranging from 600 to 1200 mesh size, followed by their washing with distilled water, ethanol and finally de-greasification by acetone. The cleaned metallic specimens were collected stored in desiccators.

Methods

Experimental methods

Because of the high precision, ease to perform and high reproducibility, the protection tendency of ME-1 and ME-2 first of all investigated by weight loss method. In order to measure the efficiency by weight loss method, the weighted metallic specimens of stated composition having dimension 2.0 cm × 0.025 cm × 2.5 cm were allotted to corrode in the 100 mL electrolytic solution of 1M HCl without and with the diverse concentrations of ME-1 and ME-2 for the immersion time of 3 h. The procedure for weight loss experiments was similar to our earlier reports [15–17]. The weight loss experimental at every studied concentration of ME-1 and ME-2 is triply performed in order to insure the reproducibility of the measurement. The weight loss parameters were calculated using following equations [15–17]:

$$C_R(mgcm^{-2}h^{-1}) = \frac{\Delta w}{A.t} \quad (1)$$

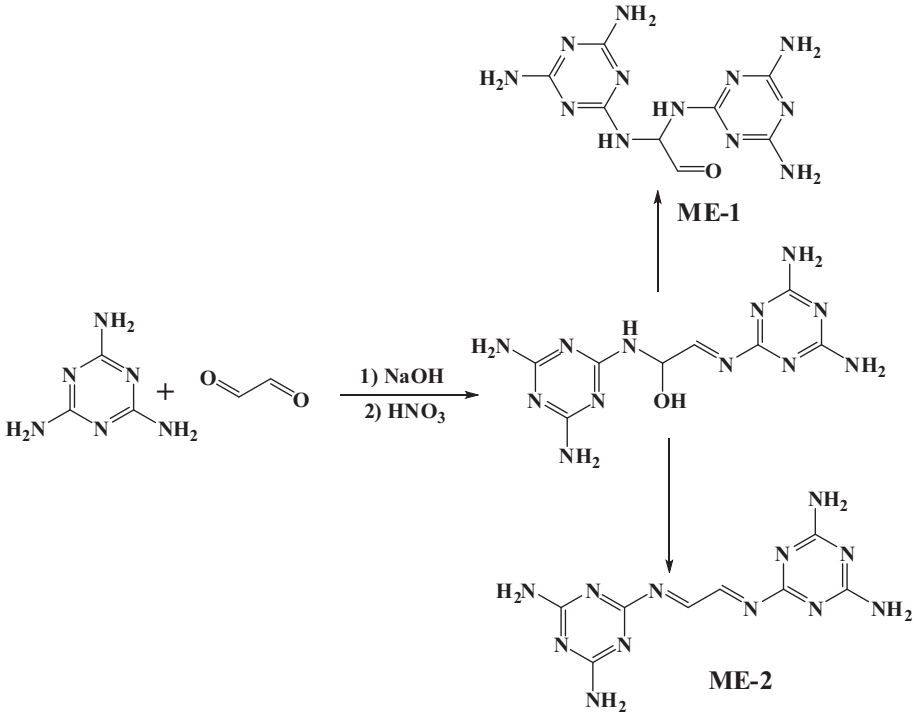

Fig. 1. Synthetic scheme for ME-1 and ME-2 inhibitor molecules.

Table 1
Chemical structures, IUPAC names, abbreviations and analytical data of the investigated inhibitor (MEs) molecules.

S. No.	IUPAC names and abbreviation	Structures	Analytical data
1	2,2-bis(4,6-diamino-1,3,5-triazin-2-ylamino)acetaldehyde (ME-1)	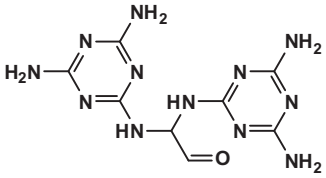	Mol. Formula: $C_8H_{12}N_{12}O$; Mol. wt.: 292.26;
2	(N^2,$N^{2'}$E,N^2,$N^{2'}$E)-N^2,$N^{2'}$-(ethane-1,2-diylidene)bis(1,3,5-triazine-2,4,6-triamine) (ME-2)	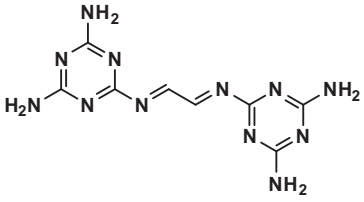	Mol. Formula: $C_8H_{10}N_{12}$; Mol. wt.: 274.12

$$\eta\% = \frac{C_{R(0)} - C_{R(i)}}{C_{R(0)}} \quad (2)$$

$$\theta = \frac{\eta\%}{100} \quad (3)$$

where, C_R ($mgcm^{-2}h^{-1}$), $\eta\%$ and θ denote the corrosion rate, the percentage of inhibition efficiency and the surface coverage, respectively. The $C_{R(i)}$ and $C_{R(0)}$ are the corrosion rate values for inhibited and non-inhibited conditions, respectively. The difference in initial and final weight of the specimens at each studied concentration is denoted by Δw, A is the surface area and t is exposure time (3hrs.).

The Gamry device (Potentiostat) that contains model G-300 and Gamry Echem Analyst 5.0 software was employed for electrochemical (OCP, PDP and EIS) studies. Procedure for the preparation of the electrodes and their nature was similar to our described reports [15–17]. The electrochemical measurements were carried out after 25 min immersion. The 25 min immersion time was sufficient to establishment of open circuit potential (OCP). The measurements using EIS method was carried out employing AC signal having 10 mV amplitude that possesses the frequency assortment of 0.01 Hz–100 kHz. Polarization resistance (Rp) values were obtained by fitting Nyquist curves of inhibited and non-inhibited metallic specimens in an equivalent circuit through which protection ability was calculated as follows [15–17]:

$$\eta\% = \left(1 - \frac{R_p}{R_{p(i)}}\right) \times 100 \quad (4)$$

In Eq. (4), R_p^0 and R_p^i are the polarization resistances under non-protected and protected cases. For PDP study the working electrode potentials were allowed to vary from −250 mV – +250 mV against the corrosion potential (E_{corr}). The linear sections of Tafel curves were extrapolated in order to derive the values of corrosion current density (i_{corr}). Using these values, the η% was derived as follows [15–17]:

$$\eta\% = \frac{i^0_{corr} - i^i_{corr}}{i^0_{corr}} \times 100 \quad (5)$$

where, i^0_{corr} and i^i_{corr} are the current densities under non-inhibited and inhibited conditions, respectively.

For surface study, cleaned and dried specimens were dipped into 100 mL 1M HCl for 3 h with and without ME-1 and ME-2 at their optimum concentration. Thereafter, specimens were washed, dried and undertaken for surface morphological measurements using AFM and SEM analyses. The SEM images of protected and non-protected specimens were taken employing SEM model Ziess Evo 50 XVP model at 2000x magnification. While, NT-MDT multimode AFM, Russia was employed for AFM analysis. The surface areas undertaken for AFM analysis were 5 mm × 5 mm.

Computational methods

The mode of adsorption by ME-1 and ME-2 on mild steel surface was studied by DFT method that was carried out on Gaussian 09 (version D.01) through B3LYP/6-31G(d) model [17–19]. Various DFT based indices were derived for neutral as well as protonated forms of ME-1 and ME-2 molecules. As per the theorem of Koopman, the values of frontier molecular orbitals can be correlated with ionization potential (I) as well as electron affinity (A) as per the Eqs. (6) and (7). Employing the magnitude of A and I, several other DFT indices like electronegativity (χ), global harness (η) and softness (σ) were computed for the both forms of ME-1 and ME-2 as per the Eqs. (8)–(10). It is well documented that metal-inhibitor bondings involve donor-acceptor phenomenon. The fraction of electron transfer (ΔN) by ME-1 and ME-2 molecules was computed as per the Eq. (11) [17–21]:

$$I = -E_{HOMO} \quad (6)$$

$$A = -E_{LUMO} \quad (7)$$

$$\eta = \frac{1}{2}(I - A) = \frac{1}{2}(-E_{HOMO} + E_{LUMO}) \quad (8)$$

$$\sigma = \frac{1}{\eta} \quad (9)$$

$$\chi = \frac{1}{2}(I + A) = \frac{1}{2}(-E_{HOMO} - E_{LUMO}) \quad (10)$$

$$\Delta N = \frac{\chi_{Fe} - \chi_{inh}}{2(\eta_{Fe} + \eta_{inh})} \quad (11)$$

where, E_{HOMO} and E_{LUMO} represent the energies of maximum unavailable orbital and lowermost vacant frontier molecular orbitals, respectively. It is important to mention that in previous studies researchers were interested to use electronegativity of the iron (7 eV) for the calculation of fraction of electron transfer (ΔN). However, recently use of work function of iron instead of electronegativity of the iron is more common and employed. It is also important to note that iron exists in its four crystalline forms that is crystalline iron, Fe (1 0 0), Fe (1 1 0) and Fe (1 1 1) having wave function (ϕ)

values of 4.26 eV, 4.64 eV, 4.52 eV and 4.74 eV, respectively . Since the wave function (ϕ) value of crystalline iron (4.26 eV) is lowest among the all form of iron therefore this value was employed for the calculation of fraction of electron transfer (ΔN) [22,23].

Results and discussions

Gravimetric study

Variation in the values of η% with ME-1 and ME-2 molecules concentrations in acidic dissolution of mild steel is designated in Table 2. From the results it can be observed that protection ability of ME-1 and ME-2 enhances with enhancing the concentrations of both molecules and acquired the highest efficiency at 125 ppm (42.80×10^{-5} M) concentration. Careful review of the Table 2 revealed that on increasing ME-1 and ME-2 from 25 ppm to 100 ppm showed significant enhancement in their protection abilities. However, on increasing their concentration from 100 to 125 ppm concentration little increase in the η% was observed. This observation revealed that 100 ppm (34.20×10^{-5} M) is optimum concentration for ME-1 and ME-2. From results it can also be seen that ME-2 showed better inhibition performance than ME-1. The higher protection ability of ME-2 as compared to ME-1 might be attributed to the presence of four additional π-electrons in form of two imine (—N═CH—) bonds in ME-2, while ME-1 has only two additional π-electrons in the form of carbonyl (—CH═O) bond. Obviously, the increase in the surface coverage values was derived on increasing the concentration of ME-1 and ME-2. However, after certain concentration when maximum surface is occupied by inhibitor molecules, further enhance in their concentration did not caused any significant increase in their inhibition efficiency [16,24–26].

The effect of temperature on protection abilities of ME-1 and ME-2 on mild steel acidic dissolution is depicted in Table 3. From the results it can be inspected that protecting abilities of both the inhibitor molecules are decreasing and thereby corresponding increase in the corrosion rate values have been observed on increasing the temperature. The decreased protection ability of ME-1 and ME-2 is attributed to the several high temperature associated phenomena like acid catalyzed molecular rearrangement, molecular fragmentation, molecular etching and desorption of adsorbed ME-1 and ME-2 inhibitor molecules. The desorption of the adsorbed ME-1 and ME-2 molecules from the metallic surface is resulted to the increased kinetic energy of the molecules at raised temperatures that ultimately results into corresponding decrease in the force constant between inhibitor molecules and metallic surface. The Arrhenius equation has been most frequently used to describe the effect of temperature metal-inhibitor interactions. The Arrhenius equation can be presented as [15–17,27]:

$$\log(C_R) = \frac{-Ea}{2.303\,RT} + \log A \tag{12}$$

where, E_a, R, T and A denote the activation energy, the universal gas constant, the absolute temperature and the Arrhenius pre-exponential factor, respectively. The E_a values were derived from the slopes of Arrhenius plots (presented as Fig. 2) of inhibited and non-inhibited metallic specimens. The calculated values of E_a were 65.72 kJ mol^{-1} and 75.27 kJ mol^{-1} for ME-1 and ME-2, respectively. Whereas, in the absence of ME-1 and ME-2 molecules E_a value was 30.50 kJ mol^{-1} only. The increased values of E_a for inhibited situations are attributed to the adsorption and development of defensive barricade by ME-1 and ME-2 molecules. The film formed by ME-1 and ME-2 molecules enhanced the energy barrier for corrosion process through their add adsorption on the surface.

The ME-1 and ME-2 interactions with metallic surface can be best signified by the adsorption isotherm model. Some common isotherms were tested to describe the adsorption behavior of the ME-1 and ME-2 molecules on the surface. The Langmuir adsorption isotherms plot is presented in Fig. 3. The values of adsorption constants (K_{ads}) at optimum concentration of ME-1 and Me-2 at different temperatures were evaluated using Langmuir adsorption isotherm equation shown below [15,16]:

$$K_{ads}C = \frac{\theta}{1-\theta} \tag{13}$$

In the equation, θ denotes the degree of surface coverage and C is the molar concentration of ME-1 and ME-2 molecules. Generally, a high value of K_{ads} is comprised with high adsorption ability. The calculated values of K_{ads} at different studied temperatures are presented in Table 3. At each temperature, ΔG_{ads} (standard free energy of adsorption) are calculated as follows [28–30]:

$$\Delta G^{\circ}_{ads} = -RT\ ln(55.5K_{ads}) \tag{14}$$

where, numerical value 55.5 denotes the concentration of concentration of water in acidic solution and other symbols have their customary meaning. The calculated values of K_{ads} are also presented in Table 3. It can be can be seen that very high negative values of ΔG_{ads} were derived for ME-1 and ME-2 which revealed that these compounds have huge adsorbing abilities [31–33]. The high values of K_{ads} for both ME-1 and ME-2 suggested that they have strong tendency of adsorption on the metallic surface [15,17,34].

Electrochemical studies

The electrochemical measurements were carried out in order to support the weight loss study. The open circuit potential (OCP) is the potential developed on the working electrode against the potential of standard or reference electrode without put on any outside current. The OCP versus time for 25 min curves after 30

Table 2
weight loss parameters derived with and without several concentrations of ME-1 and ME-2 inhibitor molecules.

Inhibitor	Conc. (ppm/M)	Wt. loss (mg)	C_R ($mgcm^{-2}h^{-1}$)	η%	θ
Blank	–	176	5.86	–	
ME-1	$25/8.56 \times 10^{-5}$	72	2.40	59.09	0.59
	$50/17.10 \times 10^{-5}$	37	1.23	78.79	0.78
	$75/25.70 \times 10^{-5}$	28	0.93	84.09	0.84
	$100/34.20 \times 10^{-5}$	15	0.50	91.47	0.91
	$125/42.80 \times 10^{-5}$	14	0.08	92.04	0.92
ME-2	$25/8.56 \times 10^{-5}$	58	1.93	67.04	0.67
	$50/17.10 \times 10^{-5}$	31	1.03	82.38	0.82
	$75/25.70 \times 10^{-5}$	18	0.60	89.77	0.89
	$100/34.20 \times 10^{-5}$	09	0.30	94.88	0.95
	$125/42.80 \times 10^{-5}$	08	0.04	95.45	0.95

Table 3
The values of corrosion rates (C_R), efficiencies (η%), adsorption constants (K_{ads}) and Gibb's free energies for corrosion of mild steel in 1M HCl at several studied temperatures.

Temp.	Blank		ME-1				ME-2			
	C_R	η%	ΔG_{ads}	$K_{ads} \times 10^4$	C_R	η%	ΔG_{ads}	$K_{ads} \times 10^4$	C_R	η%
308	5.86	–	−34.52	1.3	0.50	91.48	−35.92	2.22	0.30	94.89
318	8.20	–	−34.21	0.75	1.13	86.18	−35.25	1.10	0.80	90.24
328	12.40	–	−34.53	0.56	2.17	82.53	−35.25	0.73	1.73	86.02
338	16.60	–	−33.53	0.27	5.07	69.48	−34.26	0.35	4.20	74.69

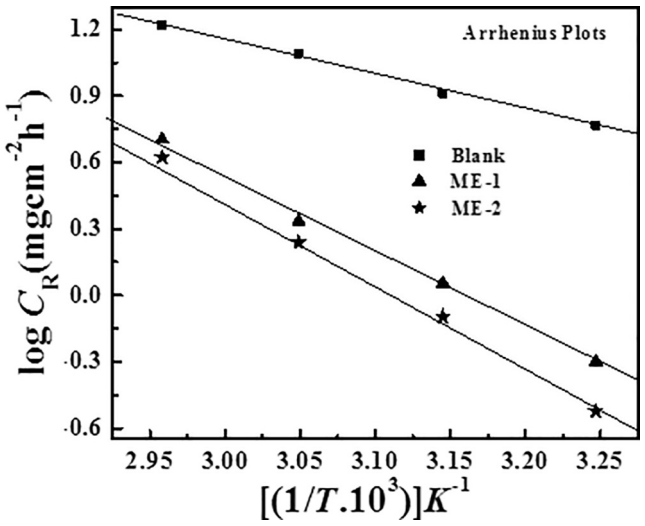

Fig. 2. Arrhenius plots for mild steel corrosive dissolution in the absence and presence of ME-1 and ME-2 inhibitor molecules.

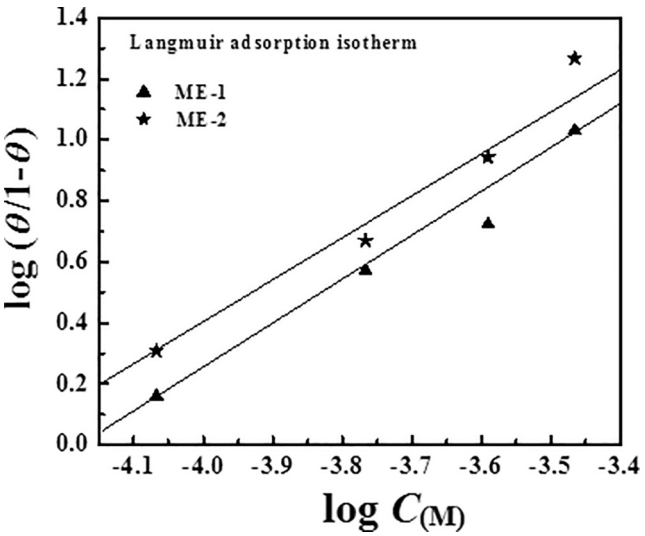

Fig. 3. Langmuir adsorption isotherm plotted for the adsorption of ME-1 and ME-2 on mild steel surface in 1M HCl.

min immersion time are presented in Fig. 4. It can be seen that the OCP versus time curves under inhibited and non-inhibited by ME-1 and ME-2 denotes the straight lines which indicate that under both situations steady state potential have been developed. The straight lines also indicate that the oxide layer present in form of Fe_2O_3 and Fe_3O_4 have been completely removed and protective or inhibitive film by ME-1 and ME-2 have been developed on the metallic surface [35–37]. It can also be seen that the OCP versus time curves in the presence of ME-1 and ME-2 are shifted towards negative or cathodic direction [38,39]. This finding suggests that although presence of ME-1 and ME-2 affect both anodic and cathodic processes, however they have relatively more effectiveness towards cathodic reactions because of their precipitation on the cathodic sites of the metallic surface.

The anodic and cathodic polarization (Tafel) curves for metallic dissolution in 1M HCl in the presence and absence of ME-1 and ME-2 are shown in Fig. 5 and polarization indices for both inhibitors are presented in Table 4. It can be seen that both cathodic and anodic reactions and processes have been affected by ME-1 and ME-2 at their several studied concentrations with substantial decrease in the corrosion current densities (i_{corr}) without fluctuating the common appearances of the Tafel curves. This observation revealed that both ME-1 and ME-2 molecules retard the corrosion process by adsorbing/ blocking the surface active sites present over the metallic surface [18,19,40]. It can be seen that corrosion potentials (E_{corr}) for Tafel curves inhibited by ME-1 and ME-2 are moved towards negative sites this finding suggests that both investigated inhibitors precipitates over cathodic region and thereby behaved as predominantly cathodic type inhibitors [41,42]. The anodic and/ or cathodic nature of inhibitor molecules (ME-1 and ME-2) can be defined on the basis of the shift in E_{corr} values of the inhibited Tafel curves as compared to the uninhibited Tafel curves (blank). From results of the polarization measurement is can also be seen that ME-2 showed better inhibition performance as compared to the ME-1 as observed by weight loss measurement.

The Bode and Nyquist plots for mild steel corrosive dissolution in aggressive acidic solution with and without ME-1 and ME-2 are presented in Figs. 6 and 7. The Nyquist plots under both situations represent single semicircle at all studied concentrations which is an ultimate consequence of single charge transfer mechanism taking place at the metal-electrolyte (1M HCl solution) interfaces. The single charge transfer mechanism is also reported by single maxima in the Bode plots observed for inhibited and non-inhibited metallic corrosion. It can be seen that diameters of the semicircle of the Nyquist plots are grater for inhibited (by ME-1 and ME-2) metallic specimens as compared to the uninhibited metallic specimen (blank). Further, the increase in the diameter of semicircles is more prominent at the higher concentrations of ME-1 and ME-2. Various impedance parameters were derived by fitting the Nyquist plots of inhibited and non-inhibited metallic specimens into an appropriate equivalent circuit described in our earlier reports [15,16]. In the proposed circuit CPE that is constant phase element has been taken under consideration at the place of pure capacitor since later one is more informative about the metal-electrolyte interactions at the interfaces as compared to the former one. The impedance of the CPE that is generally denoted by Z_{CPE} can be presented as follows [15,16]:

$$Z_{CPE} = \frac{1}{Y_0}[(j\omega)^n]^{-1} \quad (15)$$

where, the ω, Y_0, n and j denote the angular frequency, the CPE constant, the phase shift and an imaginary number, correspondingly. The n is a very significant impedance parameter in the term of

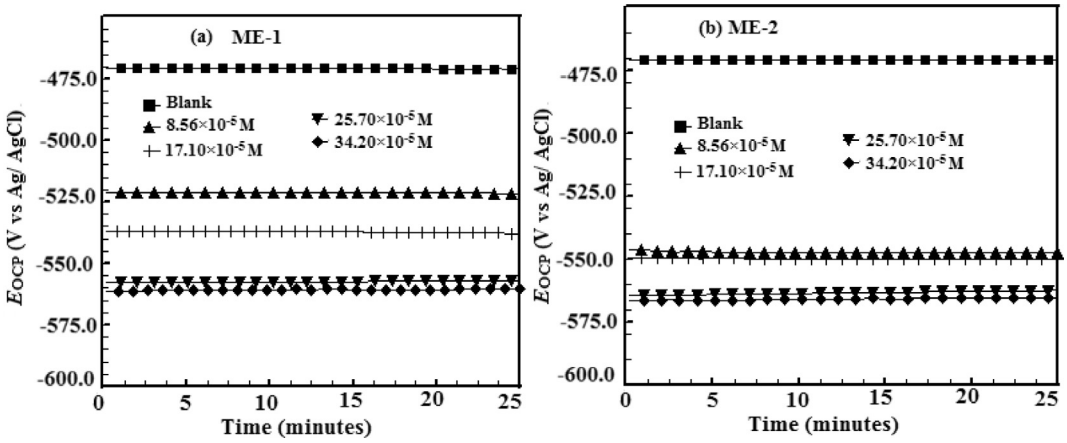

Fig. 4. Open circuit potential (OCP) versus time (minutes) curves for mild steel corrosive dissolution in 1M HCl in the absence and presence of ME-1 and ME-2 inhibitor molecules.

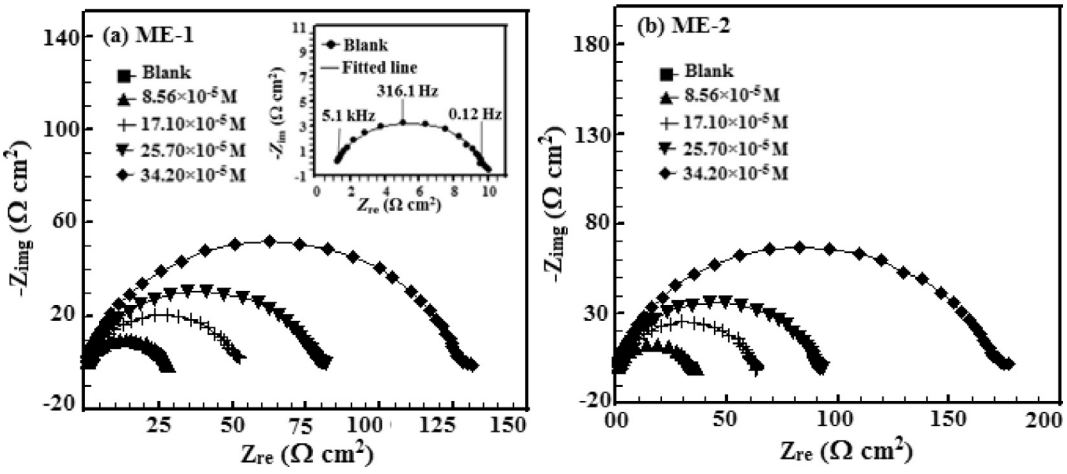

Fig. 5. Nyquist plots for corrosive dissolution of mild steel in 1M HCl with and without ME-1 and ME-2 inhibitor molecules.

Table 4
Polarization parameters derived for the corrosion of mild steel in 1M HCl with and without ME-1 and ME-2 inhibitor molecules at different concentrations.

Inhibitor	Conc. (mM/L)	E_{corr} (mV/SCE)	β_a (μA/cm^2)	$-\beta_c$ (mV/dec)	i_{corr} (mV/dec)	η%	θ
Blank	–	−445	70.5	114.6	1130	–	–
ME-1	8.56×10^{-5}	−523	69.1	107.7	461.0	59.20	0.59
	17.10×10^{-5}	−546	164.6	146.2	228.0	79.82	0.79
	25.70×10^{-5}	−526	72.2	76.3	172.0	84.77	0.84
	34.20×10^{-5}	−542	132.5	152.0	96.0	91.50	0.91
ME-2	8.56×10^{-5}	−532	127.8	97.0	386.0	65.84	0.65
	17.10×10^{-5}	−545	83.4	81.8	186.0	83.53	0.83
	25.70×10^{-5}	−453	135.1	148.8	144.0	87.25	0.87
	34.20×10^{-5}	−541	140.4	176.7	68.0	93.98	0.93

which nature of CPE is being explained. The 0, 1; −1 and 0.5 values of the n represent the resistor ($Y_0 = R$), capacitor ($Y_0 = C$), inductor ($Y_0 = 1/L$) and the Warburg impedance ($Y_0 = W$), respectively [17,19]. More so, value of n is also a measure of surface roughness or smoothness as its high magnitude is related with high surface smoothness and converse is also true. The calculated impedance parameters along with the percentage inhibition efficiencies and surface coverages are listed in Table 5. It can be seen from the results that except few selected cases the values of n are greater for the inhibited cases as compared to the uninhibited situation. This observation revealed that in the presence of ME-1 and ME-2 particularly at their higher concentrations metallic surfaces are relatively smoother than that of in their absence. It can be further seen that n values are close to unity under the both condition (inhibited and non-inhibited) indicating that CPE acts as pseudo-capacitor in the present investigation. It is well estimated that corrosion inhibition in aggressive acidic medium by organic inhibitors is attributed to their adsorption at the metal-electrolyte interfaces that results into the creation of electric double layer. The capacitance (C_{dl}) of the layer can be evaluated as [43,44]:

$$C_{dl} = Y_0 \, (\omega_{max})^{n-1} \tag{16}$$

where, ω_{max} denotes the frequency where imaginary fragment of impedance is occupied the highest (rad s-1) magnitude. The results

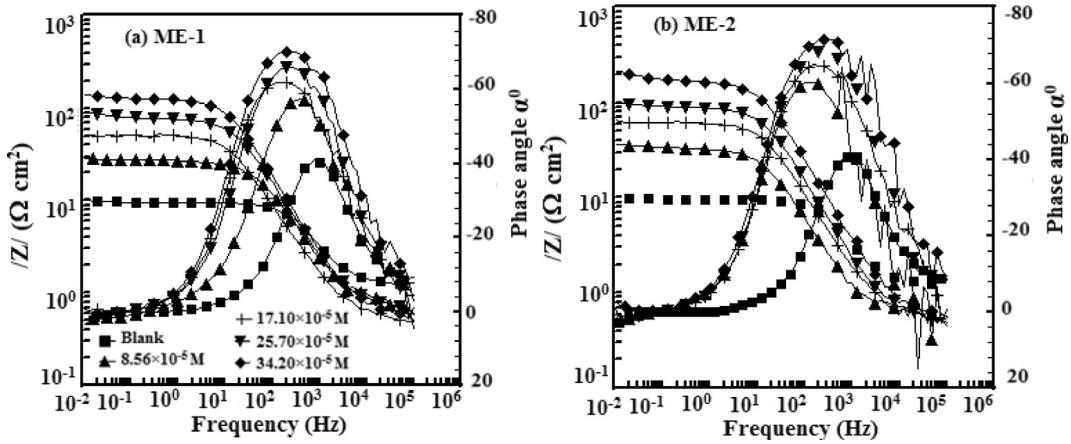

Fig. 6. Bode plots for corrosive dissolution of mild steel in 1M HCl with and without ME-1 and ME-2 inhibitor molecules.

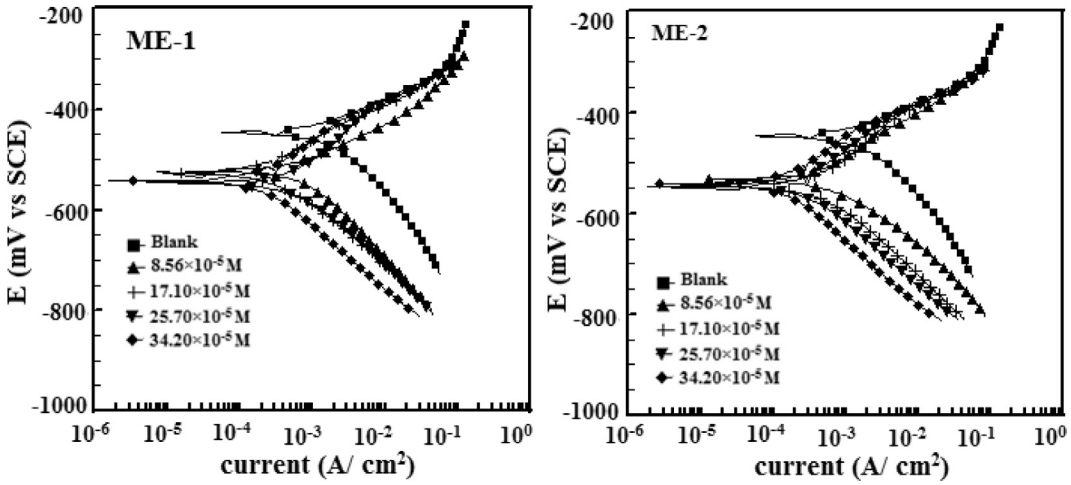

Fig. 7. Polarization for corrosive dissolution of mild steel in 1M HCl with and without ME-1 and ME-2 inhibitor molecules.

Table 5
EIS parameters derived for the corrosion of mild steel in 1M HCl with and without ME-1 and ME-2 inhibitor molecules at different concentrations.

Inhibitor	Conc (ppm)	*Rs* (Ω cm^2)	R_p (Ω cm^2)	n	C_{dl} (μF cm^{-2})	η%	θ
Blank	–	1.12	10.70	0.827	106.21	–	–
ME-1	8.56×10^{-5}	0.726	26.79	0.811	137.50	60.05	0.60
	17.10×10^{-5}	0.519	51.18	0.815	61.29	79.09	0.79
	25.70×10^{-5}	0.692	78.00	0.842	79.39	82.28	0.82
	34.20×10^{-5}	0.568	127.20	0.855	61.44	91.59	0.92
ME-2	8.56×10^{-5}	0.586	33.00	0.842	350.65	67.57	0.68
	17.10×10^{-5}	0.540	61.85	0.848	176.73	82.70	0.83
	25.70×10^{-5}	0.549	90.15	0.848	133.07	88.13	0.88
	34.20×10^{-5}	0.564	173.00	0.854	84.52	93.81	0.94

presented in Table 5 show that values of *R*ct are much higher for the cases inhibited by ME-1 and ME-2 as compared to the non-inhibited case. This finding suggests that charge transfer process has become difficult in the presence of ME-1 ad ME-2 owing to their adhering on the metal-electrolyte interfaces. Results further showed that increases in *R*ct values are even more prominent at the higher concentrations of ME-1 and ME-2. The decreased values of C_{dl} for inhibited cases revealed that thickness of the electric double layer has been improved because of the ME-1 and ME-2 adsorption at the interfaces [15–17,34]. Although, the decrease in the dielectric constant value under inhibited conditions can also decrease the values of *C*dl.

Surface studies

AFM and SEM images of metallic specimens corroded for 3 h are shown in Figs. 8 and 9. SEM and AFM images of unprotected metallic specimen is highly damaged and corroded as inspected from their highly rough surfaces with several pits and cracks like appearance. The average surface roughness of AFM image of uninhibited mild steel surface was 390 nm. However, in the presence of ME-1 and ME-2 the metallic surfaces have significantly improved as inspected from their SEM and AFM images. The average surface roughnesses were 184 nm and 146 nm for the metallic specimens protected by ME-1 and ME-2, respectively. On the basis of

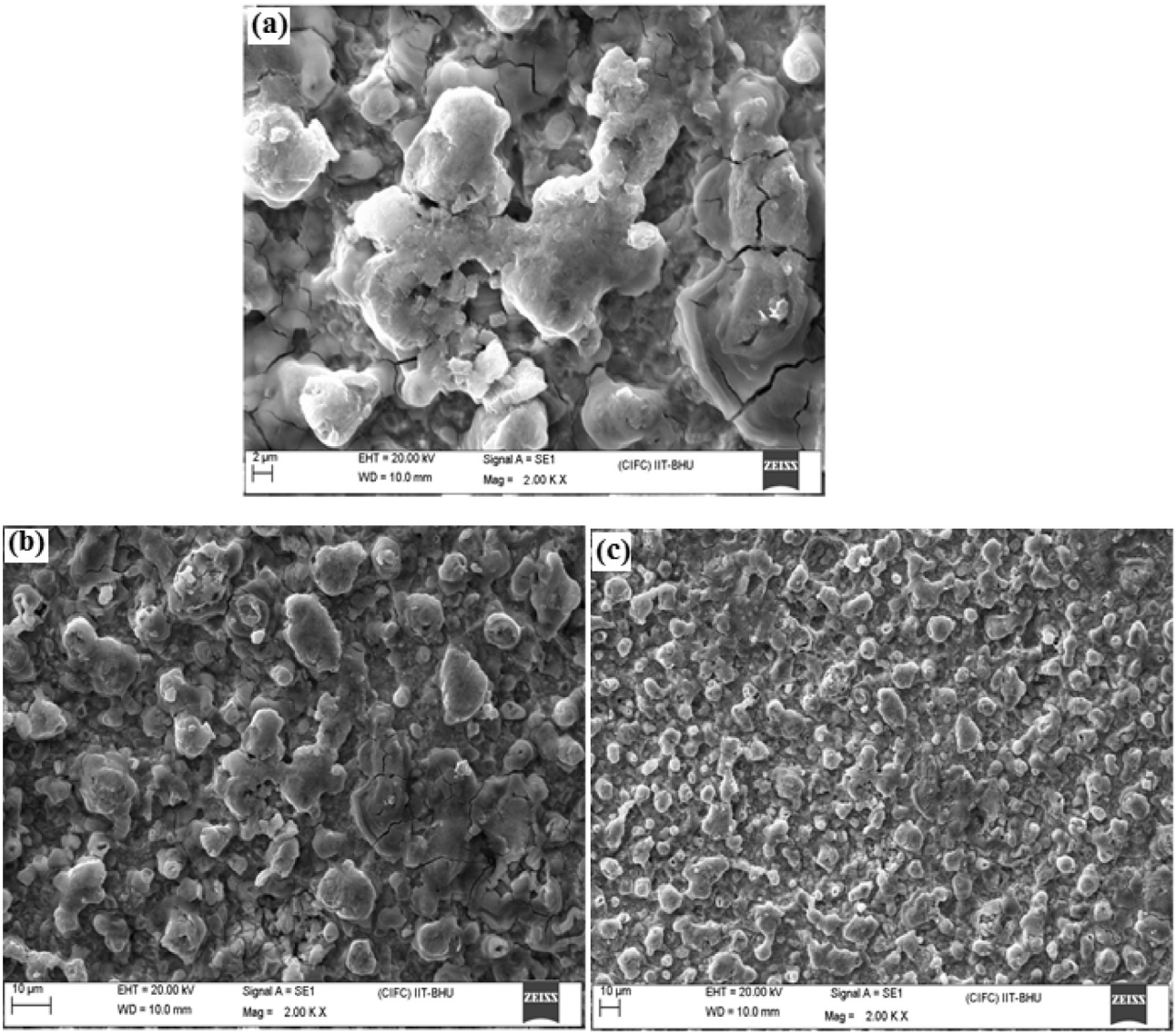

Fig. 8. SEM images of corroded mild steel surfaces for three hours immersion time in the (a) absence and presence of (b) ME-1 and (c) ME-2 molecules.

improved surface morphologies of the protected metallic specimens it can be postulated that ME-1 and ME-2 form surface film which protect metallic surface from corrosion. Further, the careful inspection of SEM and AFM images it can also be seen that surface morphology of metallic surface protected by ME-2 is smoother as compared to the surface protected by ME-1. This finding also established the trend of inhibition efficiency obtained from weight loss weight loss and electrochemical methods.

Computational studies

The frontier molecular orbitals (optimized, HOMO and LUMO) of ME-1 and ME-2 are shown in Fig. 10 and several computed DFT indices are presented in Table 6. The DFT parameters presented in the table showed good consistence with the experimental results. Obviously, interactions of corrosion inhibitors on the metallic surface involve donor-acceptor bonding and during these interactions E_{HOMO} is related with electron (charge) transferring capability of the inhibitor molecule and E_{LUMO} are consistent with the electron accepting ability of the inhibitor molecules. Therefore, a high value of E_{HOMO} and Low value of E_{LUMO} are associated strong metal-inhibitor bondings and thereby high protection ability [45–48]. Results showed that ME-2 has higher (positive) value of E_{HOMO} (−4.27 eV) than that of the ME-1 (−4.75 eV) which indicates that ME-2 is better electron donor and better corrosion inhibitor than that of ME-1 as also derived from experimental means. The values of E_{LUMO} are −0.80 eV and −2.83 eV for ME-1 and ME-2, respectively. The lower value of E_{LUMO} for ME-2 is an indicative that it is relatively better electron acceptor thereby better corrosion inhibitor as compared to the ME-1. Besides, E_{HOMO} and E_{LUMO} several other indices based on the energies of frontier molecular orbitals were computed and described in order to establish the results of experimental studies. The energy gap (ΔE; E_{LUMO}-E_{HOMO}) is perhaps the most significant reactivity factor in the term of which reactivity/ adsorption tendency of the two or more organic compounds can be described. In general, a lower energy gap between E_{LUMO} and E_{HOMO} is related with high chemical reactivity and adsorption ability/inhibition efficiency. Results presented in table revealed that ME-1 has higher value of ΔE (3.94 eV) as compared to the ΔE value of ME-2 (1.44 eV). The higher value of ΔE for ME-1

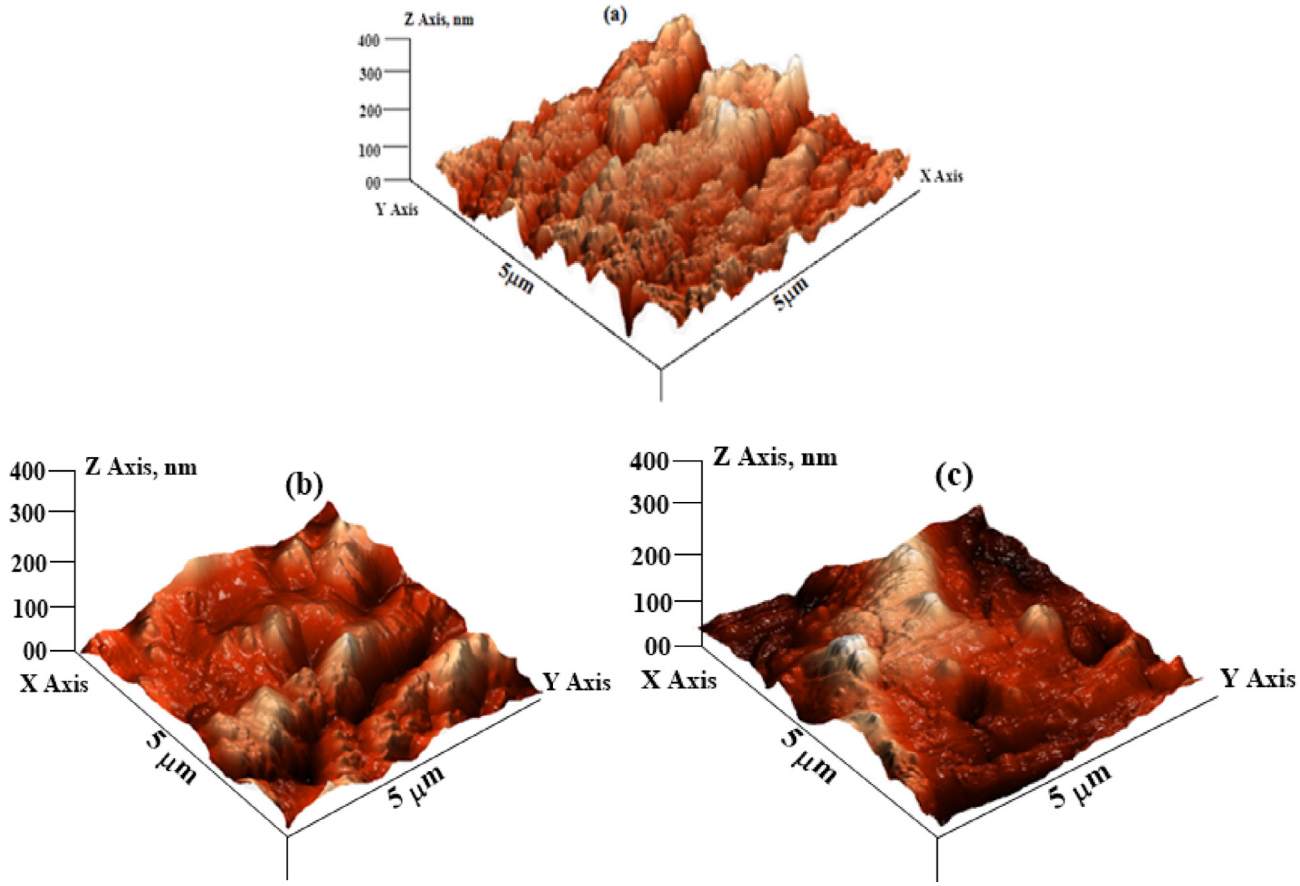

Fig. 9. AFM images of corroded mild steel surfaces for three hours immersion time in the (a) absence and presence of (b) ME-1 and (c) ME-2 molecules.

indicates that it is less reactive and poor corrosion inhibitor as compared to ME-2. The global electronegativities values for the ME-1 and ME-2 were also computed. A high value of global electronegativity (χ) suggests that undertaken compound is less potent to donate/ transfer its electron to the appropriate acceptor molecule e.g. d-orbital of the surface Fe atoms in the present case. The ME-1 and ME-2 shows the electronegativities values of 3.94 eV and 3.55 eV, respectively. The higher value of χ for ME-1 indicates that it has low ability of the electron transfer thereby acts as poor corrosion inhibitor as compared to the ME-2. Based on the values of E_{LUMO} and E_{HOMO}, global hardness (η) and softness (σ) values were also derived for ME-1 and ME-2. The high value of σ is related with high reactivity; electron donating ability, adsorption tendency and inhibition efficiency and converse is true for η [48–50]. Results showed that ME-1 has lower value of σ (0.51 eV) and higher value of η (1.97 eV) as compared to the ME-2 that suggested that ME-2 is more reactive and relatively more potent corrosion inhibitors than that of ME-1. The fraction of electron transfer (ΔN_{110}) values for ME-1 and ME-2 are given in the table. The high value of ΔN_{110} for ME-2 indicates that it is better electron donor and better corrosion inhibitor too as compared to the ME-1. During metal-inhibitor bondings, effective surface coverage takes place with the more polarizable corrosion inhibitor. The extent of inhibitor polarization can be measure with the aid of dipole moment value. An inhibitor with high value of dipole moment is assumed to be more polarizable therefore better corrosion inhibitor as compared to the inhibitor having lesser value of dipole moment. In present case ME-2 has higher value of dipole moment (6.43 Debye) as compared to ME-1 (2.35 Debye). This finding suggests that ME-2 has better tendency of the polarization thereby acts as better adsorbate on the metallic surface relative to the ME-1. On the basic of above discussion it can be concluded that DFT study provide good support to the experimental results and findings.

It is well documented that the heteroatoms of the organic compounds undergo protonation in the aggressive acidic media therefore they generally exist in their cationic form. Considering this hypothesis, the DFT study was also performed on the mono-protonated form of ME-1 and ME-2. The optimized, HOMO and LUMO frontier molecular orbital pictures of the ME-1 and ME-2 are presented in Fig. 11. From the figure it can be seen that HOMO protonated forms of ME molecules are located over one triazine ring while on the second triazine ring mainly LUMO is located. This observation suggests that one of the triazine ring acts as electron donor while the second ring acts as electron acceptor during metal-inhibitor interactions. The molecular electrostatic potential (MEP) is method to see the electron density visibly. The red (negative) fragments of the MEP represent the sites for nucleophilic attack while blue (positive) fragments denote the sites for electrophilic attack. The red (nucleophilic) and blue (electrophilic) regions correspond to HOMO and LUMO electron distribution of the inhibitor molecules, respectively. It can be seen form the MEP map of the melamine derivatives that red region of the manuscript mainly localized over the electron rich part of the molecules which correspond that correspond to the HOMO. Similarly blue area is mainly located over the electron deficient part of the melamine derivatives which correspond to the LUMO. The results showed that MEP maps support the HOMO

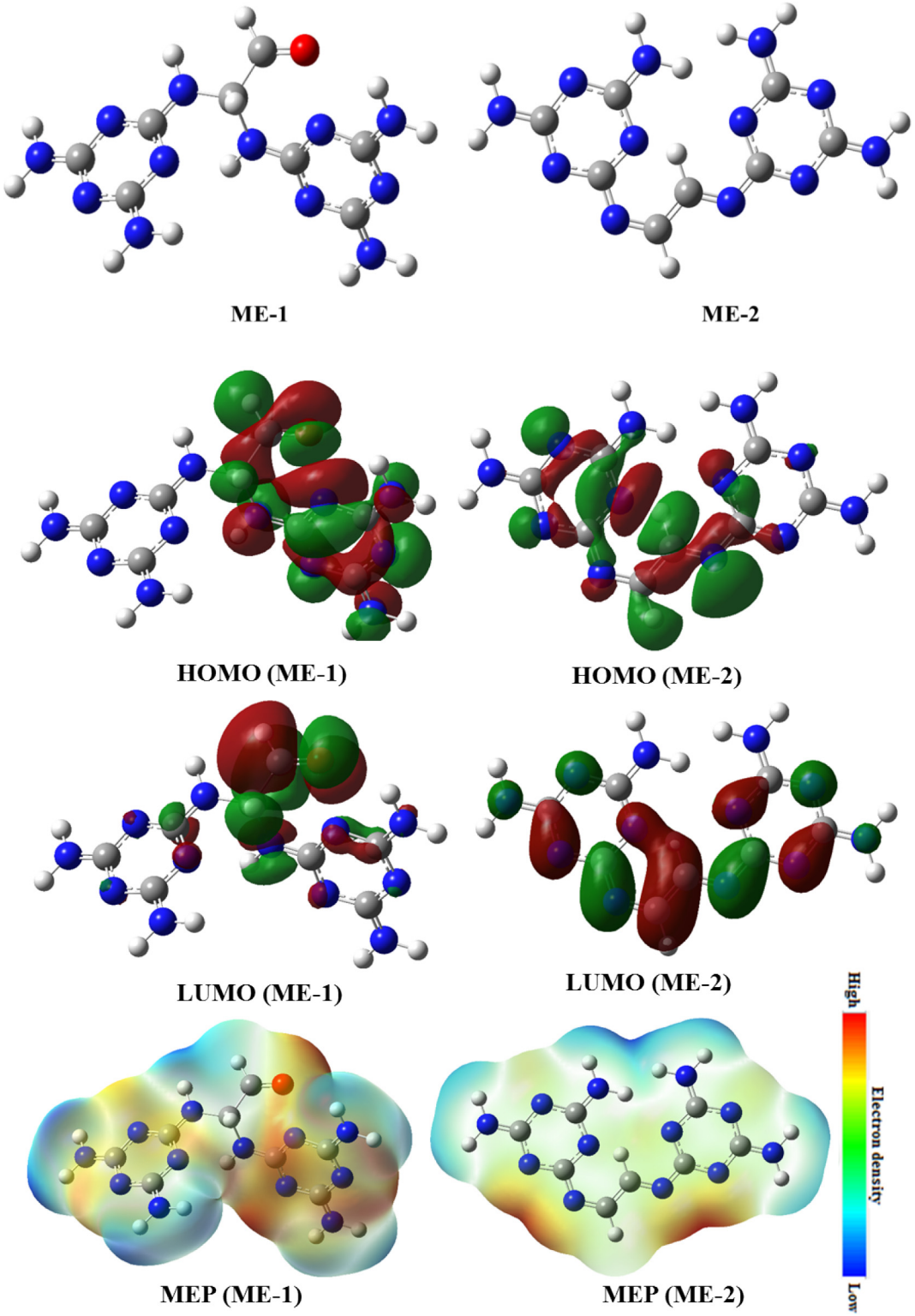

Fig. 10. Frontier molecular orbital (HOMOs and LUMOs) and molecular electrostatic potential (MEP) of neutral form of ME-1 and ME-2 inhibitor molecules.

and LUMO electron distribution. The results presented for protonated form of ME-1 and ME-2 in Table 6 revealed that E_{HOMO} are increasing on going ME-1 to ME-2, while the E_{LUMO} values are decreasing in the same order. These finding support the trend of experimental inhibition efficiency. Similarly other DFT based parameters derived for protonated form of ME molecules are consisted with the trend of DFT indices computed for their neutral form.

Table 6
DFT parameters derived for neutral as well as protonated forms of ME-1 and ME-2 inhibitor molecules.

Inhibitors↓	Parameters→							
	E_{HOMO} (eV)	E_{LUMO} (eV)	ΔE (eV)	η (eV)	σ (eV)	χ (eV)	ΔN_{110}	μ (Debye)
Neutral form								
ME-1	−4.75	−0.80	3.94	1.97	0.51	3.94	−0.105	2.35
ME-2	−4.27	−2.83	1.44	0.72	1.38	3.55	0.229	6.43
Protonated form								
ME-1	−7.31	−5.20	2.10	1.05	0.95	6.26	−1.133	15.46
ME-2	−7.38	−6.28	1.09	0.55	1.83	6.83	−2.682	17.02

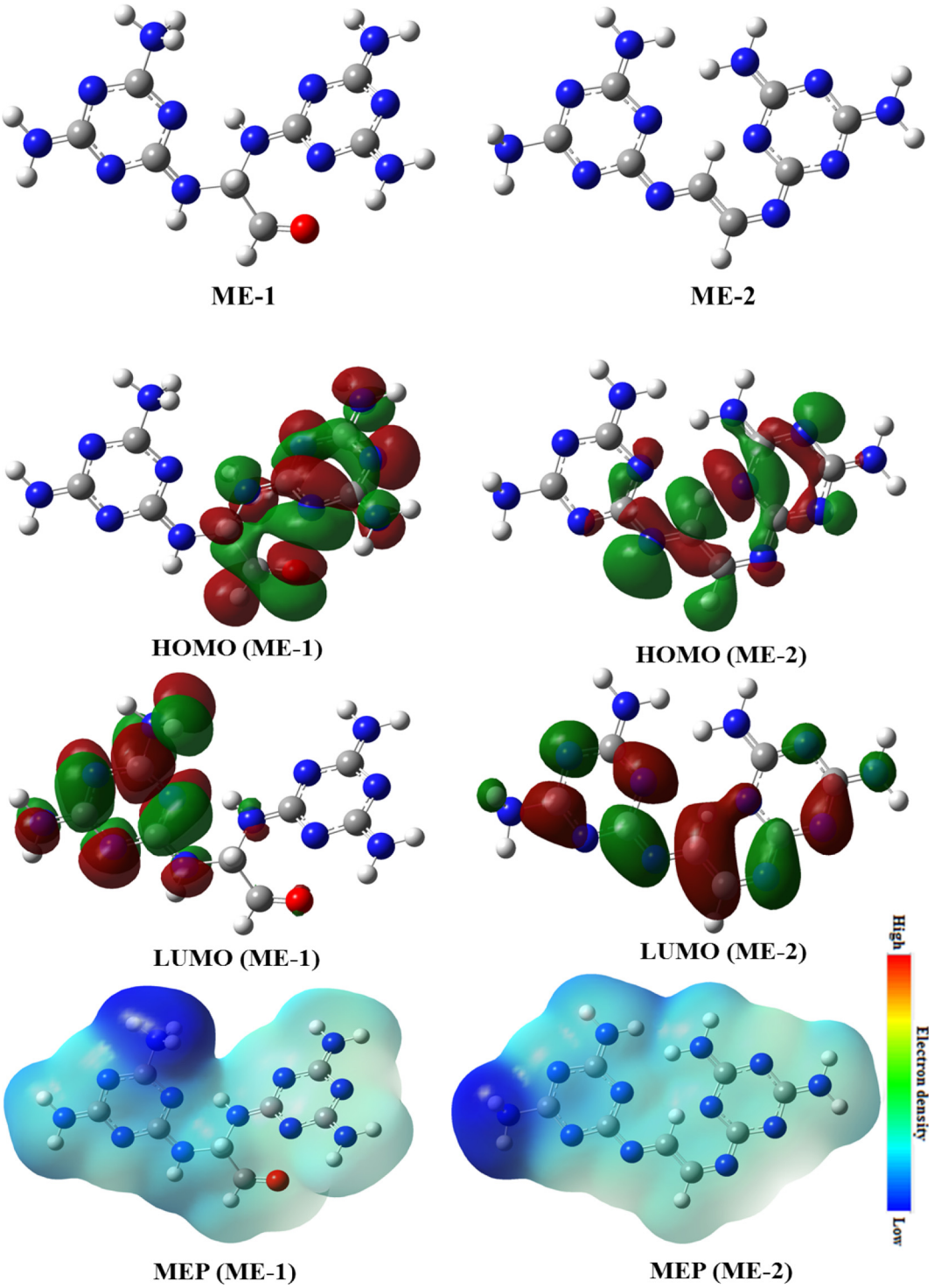

Fig. 11. Frontier molecular orbital (HOMOs and LUMOs) and molecular electrostatic potential (MEP) of protonated form of ME-1 and ME-2 inhibitor molecules.

Conclusions

The inhibition effect of tow melamine based organic compounds namely, 2,2-bis(4,6-diamino-1,3,5-triazin-2-ylamino)acet aldehyde (ME-1) and (N^2,$N^{2'}$E,N^2,$N^{2'}$E)-N^2,$N^{2'}$-(ethane-1,2-diyli dene)bis(1,3,5-triazine-2,4,6-triamine) (ME-2) tested in the present study and it was concluded that:

(i) Both ME-1 and ME-2 behaved as good inhibitors for mild steel corrosion in 1M HCl.
(ii) Their protection ability enhances with their concentration and maximum efficiencies of 92.04% and 95.45% were derived for ME-1 and ME-2, respectively.
(iii) EIS results revealed that both ME-1 and ME-3 adsorb at metal-electrolyte (1M HCl) and enhance the charge transfer resistance (R_{ct}).
(iv) The adsorption of the ME-1 and ME-2 on the metallic surface obeyed the Langmuir adsorption isotherm model.
(v) Polarization study revealed that ME-1 and ME-2 act as predominantly cathodic type inhibitors.
(vi) AFM and SEM images showed that presence of ME-1 and ME-2 in the corrosive medium (1M HCl) enhances the surface smoothness owing to their adsorption at the metallic surface.
(vii) DFT studies carried out for neutral as well as protonated forms of ME-1 and ME-2 provide good support the experimental results and it established that ME-2 interact more strongly with the metallic surface as compared to the ME-1.

Acknowledgments

C. Verma thankfully acknowledges North-West University, Mafikeng Campus, South Africa for providing financial support for the study and postdoctoral fellowship.

Appendix A. Supplementary data

Supplementary data associated with this article can be found, in the online version, at https://doi.org/10.1016/j.rinp.2018.02.018.

References

[1] Yousefi A, Javadian S, Dalir N, Kakemam J, Akbari J. Imidazolium-based ionic liquids as modulators of corrosion inhibition of SDS on mild steel in hydrochloric acid solutions: experimental and theoretical studies. RSC Adv 2015;5:11697–713.
[2] Tourabi M, Nohair K, Traisnel M, Jama C, Bentiss F. Electrochemical and XPS studies of the corrosion inhibition of carbon steel in hydrochloric acid pickling solutions by 3, 5-bis (2-thienylmethyl)-4-amino-1, 2, 4-triazole. Corros Sci 2013;75:123–33.
[3] Sastri VS. Green corrosion inhibitors: theory and practice. John Wiley & Sons; 2012.
[4] Fekry A, Mohamed RR. Acetyl thiourea chitosan as an eco-friendly inhibitor for mild steel in sulphuric acid medium. Electrochim Acta 2010;55:1933–9.
[5] Gupta RK, Malviya M, Verma C, Quraishi M. Aminoazobenzene and diaminoazobenzene functionalized graphene oxides as novel class of corrosion inhibitors for mild steel: experimental and DFT studies. Mater Chem Phys 2017;198:360–73.
[6] Gupta RK, Malviya M, Verma C, Gupta NK, Quraishi M. Pyridine-based functionalized graphene oxides as a new class of corrosion inhibitors for mild steel: an experimental and DFT approach. RSC Adv 2017;7:39063–74.
[7] Al-Otaibi M, Al-Mayouf A, Khan M, Mousa A, Al-Mazroa S, Alkhathlan H. Corrosion inhibitory action of some plant extracts on the corrosion of mild steel in acidic media. Arabian J Chem 2014;7:340–6.
[8] Umoren S, Ogbobe O, Igwe I, Ebenso E. Inhibition of mild steel corrosion in acidic medium using synthetic and naturally occurring polymers and synergistic halide additives. Corros Sci 2008;50:1998–2006.
[9] Liao LL, Mo S, Luo HQ, Feng YJ, Yin HY, Li NB. Relationship between inhibition performance of melamine derivatives and molecular structure for mild steel in acid solution. Corros Sci 2017.
[10] Yadav M, Kumar S, Tiwari N, Bahadur I, Ebenso EE. Experimental and quantum chemical studies of synthesized triazine derivatives as an efficient corrosion inhibitor for N80 steel in acidic medium. J Mol Liq 2015;212:151–67.
[11] El-Sayed A-R, Mohran HS, El-Lateef HMA. The inhibition effect of 2, 4, 6-tris (2-pyridyl)-1, 3, 5-triazine on corrosion of tin, indium and tin–indium alloys in hydrochloric acid solution. Corros Sci 2010;52:1976–84.
[12] Hu Z, Meng Y, Ma X, Zhu H, Li J, Li C, Cao D. Experimental and theoretical studies of benzothiazole derivatives as corrosion inhibitors for carbon steel in 1M HCl. Corros Sci 2016;112:563–75.
[13] Sharifi Z, Pakshir M, Mohamadi S. Investigation of synthesized sulfonated melamine formaldehyde as a novel corrosion inhibitor for mild steel in saline environment. J Mater Eng Perform 2015;24:664–9.
[14] León G, Paret N, Fankhauser P, Grenno D, Erni P, Ouali L, Berthier D. Formaldehyde-free melamine microcapsules as core/shell delivery systems for encapsulation of volatile active ingredients. RSC Adv 2017;7:18962–75.
[15] Verma C, Ebenso E, Bahadur I, Obot I, Quraishi M. 5-(Phenylthio)-3H-pyrrole-4-carbonitriles as effective corrosion inhibitors for mild steel in 1 M HCl: experimental and theoretical investigation. J Mol Liq 2015;212:209–18.
[16] Verma C, Olasunkanmi L, Obot I, Ebenso EE, Quraishi M. 5-Arylpyrimido-[4, 5-b] quinoline-diones as new and sustainable corrosion inhibitors for mild steel in 1 M HCl: a combined experimental and theoretical approach. RSC Adv 2016;6:15639–54.
[17] Verma C, Olasunkanmi LO, Ebenso EE, Quraishi M, Obot I. Adsorption behavior of glucosamine-based, pyrimidine-fused heterocycles as green corrosion inhibitors for mild steel: experimental and theoretical studies. J Phys Chem C 2016;120:11598–611.
[18] Singh P, Ebenso EE, Olasunkanmi LO, Obot I, Quraishi M. Electrochemical, theoretical, and surface morphological studies of corrosion inhibition effect of green naphthyridine derivatives on mild steel in hydrochloric acid. J Phys Chem C 2016;120:3408–19.
[19] Olasunkanmi LO, Obot IB, Kabanda MM, Ebenso EE. Some quinoxalin-6-yl derivatives as corrosion inhibitors for mild steel in hydrochloric acid: experimental and theoretical studies. J Phys Chem C 2015;119:16004–19.
[20] Saha SK, Ghosh P, Hens A, Murmu NC, Banerjee P. Density functional theory and molecular dynamics simulation study on corrosion inhibition performance of mild steel by mercapto-quinoline Schiff base corrosion inhibitor. Physica E 2015;66:332–41.
[21] Obot I, Macdonald D, Gasem Z. Density functional theory (DFT) as a powerful tool for designing new organic corrosion inhibitors. Part 1: an overview. Corros Sci 2015;99:1–30.
[22] Mishra A, Verma C, Lgaz H, Srivastava V, Quraishi M, Ebenso EE. Synthesis, characterization and corrosion inhibition studies of N-phenyl-benzamides on the acidic corrosion of mild steel: experimental and computational studies. J Mol Liq 2018;251:317–32.
[23] Saha SK, Banerjee P. A theoretical approach to understand the inhibition mechanism of steel corrosion with two aminobenzonitrile inhibitors. RSC Adv 2015;5:71120–30.
[24] Jiang X, Zheng Y, Ke W. Effect of flow velocity and entrained sand on inhibition performances of two inhibitors for CO 2 corrosion of N80 steel in 3% NaCl solution. Corros Sci 2005;47:2636–58.
[25] Satapathy A, Gunasekaran G, Sahoo S, Amit K, Rodrigues P. Corrosion inhibition by *Justicia gendarussa* plant extract in hydrochloric acid solution. Corros Sci 2009;51:2848–56.
[26] Gunasekaran G, Chauhan L. Eco friendly inhibitor for corrosion inhibition of mild steel in phosphoric acid medium. Electrochim. Acta 2004;49:4387–95.
[27] Khaled K, El-Maghraby A. Experimental, Monte Carlo and molecular dynamics simulations to investigate corrosion inhibition of mild steel in hydrochloric acid solutions. Arabian J Chem 2014;7:319–26.
[28] Laamari R, Benzakour J, Berrekhis F, Abouelfida A, Derja A, Villemin D. Corrosion inhibition of carbon steel in hydrochloric acid 0.5 M by hexa methylene diamine tetramethyl-phosphonic acid. Arabian J Chem 2011;4:271–7.
[29] Loto RT, Loto CA, Joseph O, Olanrewaju G. Adsorption and corrosion inhibition properties of thiocarbanilide on the electrochemical behavior of high carbon steel in dilute acid solutions. Results Phys 2016;6:305–14.
[30] El Rehim SA, Sayyah S, El-Deeb M, Kamal S, Azooz R. Adsorption and corrosion inhibitive properties of P (2-aminobenzothiazole) on mild steel in hydrochloric acid media. Int J Ind Chem 2016;7:39–52.
[31] Hamdy A, El-Gendy NS. Thermodynamic, adsorption and electrochemical studies for corrosion inhibition of carbon steel by henna extract in acid medium. Egypt J Pet 2013;22:17–25.
[32] Mashuga ME, Olasunkanmi LO, Adekunle AS, Yesudass S, Kabanda MM, Ebenso EE. Adsorption, thermodynamic and quantum chemical studies of 1-hexyl-3-methylimidazolium based ionic liquids as corrosion inhibitors for mild steel in HCl. Materials 2015;8:3607–32.
[33] Loto RT. Study of the synergistic effect of 2-methoxy-4-formylphenol and sodium molybdenum oxide on the corrosion inhibition of 3CR12 ferritic steel in dilute sulphuric acid. Results Phys 2017;7:769–76.
[34] Verma C, Olasunkanmi LO, Obot I, Ebenso EE, Quraishi M. 2, 4-Diamino-5-(phenylthio)-5 H-chromeno [2, 3-b] pyridine-3-carbonitriles as green and effective corrosion inhibitors: gravimetric, electrochemical, surface morphology and theoretical studies. RSC Adv 2016;6:53933–48.

[35] Bentiss F, Lagrenee M, Traisnel M, Hornez J. The corrosion inhibition of mild steel in acidic media by a new triazole derivative. Corros Sci 1999;41:789–803.
[36] Lai C, Xie B, Zou L, Zheng X, Ma X, Zhu S. Adsorption and corrosion inhibition of mild steel in hydrochloric acid solution by S-allyl-O, O′-dialkyldithiophosphates. Results Phys 2017;7:3434–43.
[37] Yadav M, Sinha R, Kumar S, Sarkar T. Corrosion inhibition effect of spiropyrimidinethiones on mild steel in 15% HCl solution: insight from electrochemical and quantum studies. RSC Adv 2015;5:70832–48.
[38] Chi-Ucán SL, Castillo-Atoche A, Castro Borges P, Manzanilla-Cano JA, González-García G, Patiño R, Díaz-Ballote L. Inhibition effect of glycerol on the corrosion of copper in NaCl solutions at different pH values. J Chem 2014;2014:1–10.
[39] Pandey A, Singh B, Verma C, Ebenso EE. Synthesis, characterization and corrosion inhibition potential of two novel Schiff bases on mild steel in acidic medium. RSC Adv 2017;7:47148–63.
[40] Qu J-E, Guo X, Chen Z. Adsorption behavior of dodecylamine on copper–nickel alloy surface in NaCl solutions studied by electrochemical methods and AFM. Mater Chem Phys 2005;93:388–94.
[41] Hong-bo F, Hui-long W, Xing-peng G, Jia-shen Z. Corrosion inhibition mechanism of carbon steel by sodium N, N-diethyl dithiocarbamate in hydrochloric acid solution. Anti-Corrosion Methods Mater 2002;49:270–6.
[42] Desai M, Desai M, Shah C, Desai S. Schiff bases as corrosion inhibitors for mild steel in hydrochloric acid solutions. Corros Sci 1986;26:827–37.
[43] Xu B, Yang W, Liu Y, Yin X, Gong W, Chen Y. Experimental and theoretical evaluation of two pyridinecarboxaldehyde thiosemicarbazone compounds as corrosion inhibitors for mild steel in hydrochloric acid solution. Corros Sci 2014;78:260–8.
[44] Benabdellah M, Tounsi A, Khaled K, Hammouti B. Thermodynamic, chemical and electrochemical investigations of 2-mercapto benzimidazole as corrosion inhibitor for mild steel in hydrochloric acid solutions. Arabian J Chem 2011;4:17–24.
[45] El-Haddad MN, Elattar KM. Synthesis, characterization and inhibition effect of new antipyrinyl derivatives on mild steel corrosion in acidic solution. Int J Ind Chem 2015;6:105–17.
[46] Haque J, Srivastava V, Verma C, Lgaz H, Salghi R, Quraishi M. Methyl-N, N, N-trioctylammonium chloride as a novel and green corrosion inhibitor for mild steel in an acid chloride medium: electrochemical, DFT and MD studies. New J Chem 2017;41:13647–62.
[47] Fouda A, Ismail M, Abousalem AS, Elewady G. Experimental and theoretical studies on corrosion inhibition of 4-amidinophenyl-2, 2′-bifuran and its analogues in acidic media. RSC Adv 2017;7:46414–30.
[48] Kadhim A, Al-Okbi AK, Jamil DM, Qussay A, Al-Amiery AA, Gaaz TS, Kadhum AAH, Mohamad AB, Nassir MH. Experimental and theoretical studies of benzoxazines corrosion inhibitors. Results Phys 2017;7:4013–9.
[49] Zarrouk A, Hammouti B, Dafali A, Bouachrine M, Zarrok H, Boukhris S, Al-Deyab SS. A theoretical study on the inhibition efficiencies of some quinoxalines as corrosion inhibitors of copper in nitric acid. J Saudi Chem Soc 2014;18:450–5.
[50] Obi-Egbedi N, Obot I, El-Khaiary MI. Quantum chemical investigation and statistical analysis of the relationship between corrosion inhibition efficiency and molecular structure of xanthene and its derivatives on mild steel in sulphuric acid. J Mol Struct 2011;1002:86–96.